Rapid synthesis of $La_{0.9}Sr_{0.1}Ga_{0.8}Mg_{0.2}O_{3-\delta}$ electrolyte by a CO_2 laser and its electric properties for intermediate temperature solid state oxide full cells

J. Zhang, E.J. Liang*, X.H. Zhang

School of Physical Science & Engineering and Key Laboratory of Materials Physics of Ministry of Education of China, Zhengzhou University, No. 75, North Daxue Road, Zhengzhou 450052, China

ABSTRACT

A laser rapid solidification (LRS) method has been developed for the synthesis of $La_{0.9}Sr_{0.1}Ga_{0.8}Mg_{0.2}O_{3-\delta}$ (LSGM), an excellent electrolyte for solid oxide fuel cells. It is shown that pure perovskite LSGM phase can be produced within a few seconds with this method under optimized synthetic conditions and it solidified in densely packed and relatively ordered ridge-like blocks with a relative density of 98.5%. The unique microstructures are attributed to the oriented crystalline growth in the molten pool dictated by heat transfer directions. It is found that the samples synthesized by LRS exhibit superior electrical properties for fuel cell applications to those by solid state reactions. The conductivities of 0.027, 0.079 and $0.134\,S\,cm^{-1}$ measured at 600, 700 and 800 °C, respectively are much higher than those of the samples synthesized by solid state reactions with similar purity and density.

© 2010 Elsevier B.V. All rights reserved.

1. Introduction

Solid oxide fuel cells (SOFCs) can directly convert chemical energy of fuels to electrical energy with advantages of high electrical efficiency, fuel versatility, and low pollution emissions [1]. Conventional SOFCs with Y_2O_3-stabilized ZrO_2 (YSZ) electrolytes require high operating temperatures (800–1000 °C) and serious problems may arise such as mechanical stress due to mismatch in thermal expansion, interfacial diffusion and/or reaction between electrolyte and electrode materials and difficulty in sealing. These problems increase manufacturing cost and reduce the reliability of the fuel cells [2]. In order to reduce the operating temperature, many efforts have been devoted to develop novel electrolytes for intermediate temperature (600–800 °C) SOFCs. The perovskite oxide, strontium- and magnesium-doped $LaGaO_3$ (LSGM), exhibits a higher ionic conductivity ($\sim$0.10 S cm^{-1} at 800 °C [3,4]) than YSZ over a wide range of oxygen partial pressure. These superior electrical and stable properties make $LaGaO_3$-based oxides the most promising candidates as electrolytes for intermediate temperature SOFCs.

LSGM powders were generally synthesized by solid state reactions [5–9] or wet chemical routes [10–19]. However, the solid state reactions suffer from the chemical in-homogeneity, severe

time and energy wasting while the wet chemical methods require expensive metal alkoxide precursors, great care in mixing the precursors to achieve the desired stoichiometry and tedious pretreatment before the final calcinating step. Due to the narrow composition range for the stability of the perovskite phase, small deviations from the ideal composition would result in secondary phases which deteriorate the performance of the electrolyte [19,20]. The synthesis of a pure single phase material of LSGM is a rather difficult task. Therefore, it is necessary to explore new and rapid synthetic methods.

The synthesis of pure bulk materials with laser rapid solidification (LRS) is a relatively new technique [21–25]. In this paper, laser rapid solidification was employed to synthesize LSGM electrolyte and the microstructure and electrical properties of the samples synthesized by laser were studied and compared to the samples synthesized by solid state reactions. It is shown that high purity LSGM electrolyte can be produced within a few seconds with this technique which simplifies the processing procedures and shortens the sintering time greatly. Further investigations on the samples reveal that the LSGM material synthesized by the laser synthetic route exhibits unique microstructure and superior electric properties for SOFCs.

2. Experimental

$La_{0.9}Sr_{0.1}Ga_{0.8}Mg_{0.2}O_{3-\delta}$ (LSGM) samples were prepared with starting materials of Ga_2O_3 (99.99%), La_2O_3 (99.99%), MgO (98%)

* Corresponding author. Tel.: +86 371 67767838; fax: +86 371 67766629.
*E-mail address:* ejliang@zzu.edu.cn (E.J. Liang).
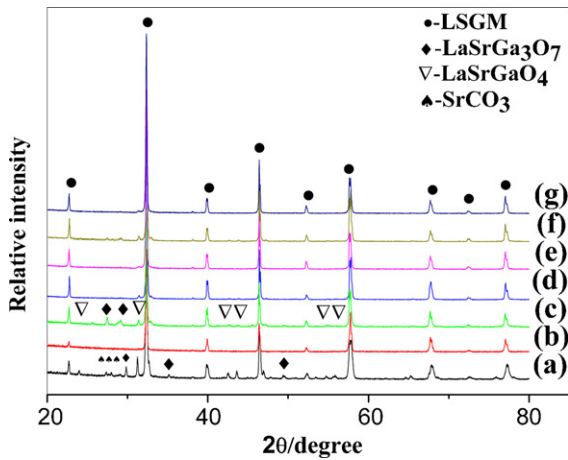
Fig. 1. XRD patterns of LSGM powders synthesized by (a) solid state reaction at respectively 1200 °C for 24 h and at 1400 °C for 6 h (SSR1); (b) solid state reaction at respectively 1250 °C for 10 h, 1500 °C for 6 h and 1600 °C for 2 h (SSR2); (c–g) laser rapid solidification (LRS) with respectively 800, 1000 and 1100 W laser powers at 1 mm s^{-1} scan speed, and 1100 W laser power at 2 and 0.6 mm s^{-1} scan speed.

and SrCO$_3$ (99%). MgO and La$_2$O$_3$ were fired at 1000 °C for 7 h before weighting to decompose carbonate and hydroxide impurities. The absence of impurities in the reagents was checked by X-ray diffraction (XRD). The mixtures were ground in a mortar for 2 h and then pressed into cuboid bars (40 mm × 5 mm × 5 mm) by uni-axial cold press with a steel mould at a pressure of 10 MPa and dried for 2 h at 100 °C in a baking oven before sintering. The synthesis was performed by using a 5 kW continuous-wave CO$_2$ laser. The laser beam was striking onto a bar placed at a distance where the defocus length was set to 120 mm. The beam spot on the sample was approximately 12 mm in diameter. As the laser beam moves ahead along the length direction, the synthesized sample behind cools naturally and rapidly to room temperature. Such cooling process can be regarded as rapid solidification. In order to optimize the synthesis conditions, we changed the scan speed from 0.6 to 3 mm s^{-1} at a fixed laser power and altered the laser power from 700 to 1100 W at a fixed scan speed. For comparison, two series of samples were prepared by conventional solid state reactions with pressed bars or pellets, one by calcinating at 1200 °C for 24 h and then sintering at 1400 °C for 6 h with intermediate grinding (denoted as SSR1) and another by calcinating at 1250 °C for 10 h and then sintering at 1500 °C for 6 h and at 1600 °C for 2 h with intermediate
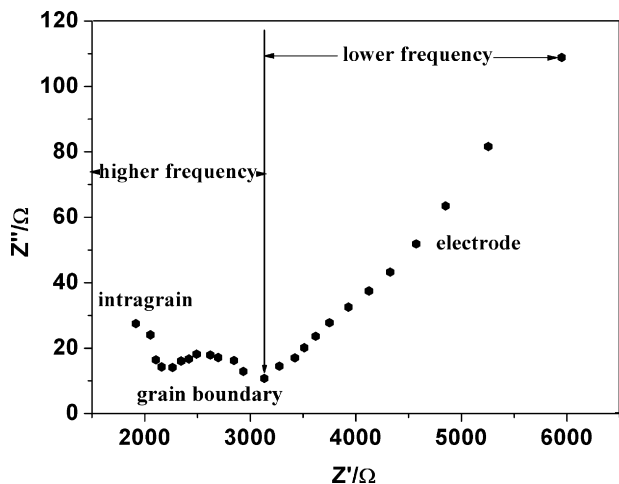
Fig. 2. Representative AC impedance spectra at 250 °C of the LSGM prepared by solid state reaction (SSR2).
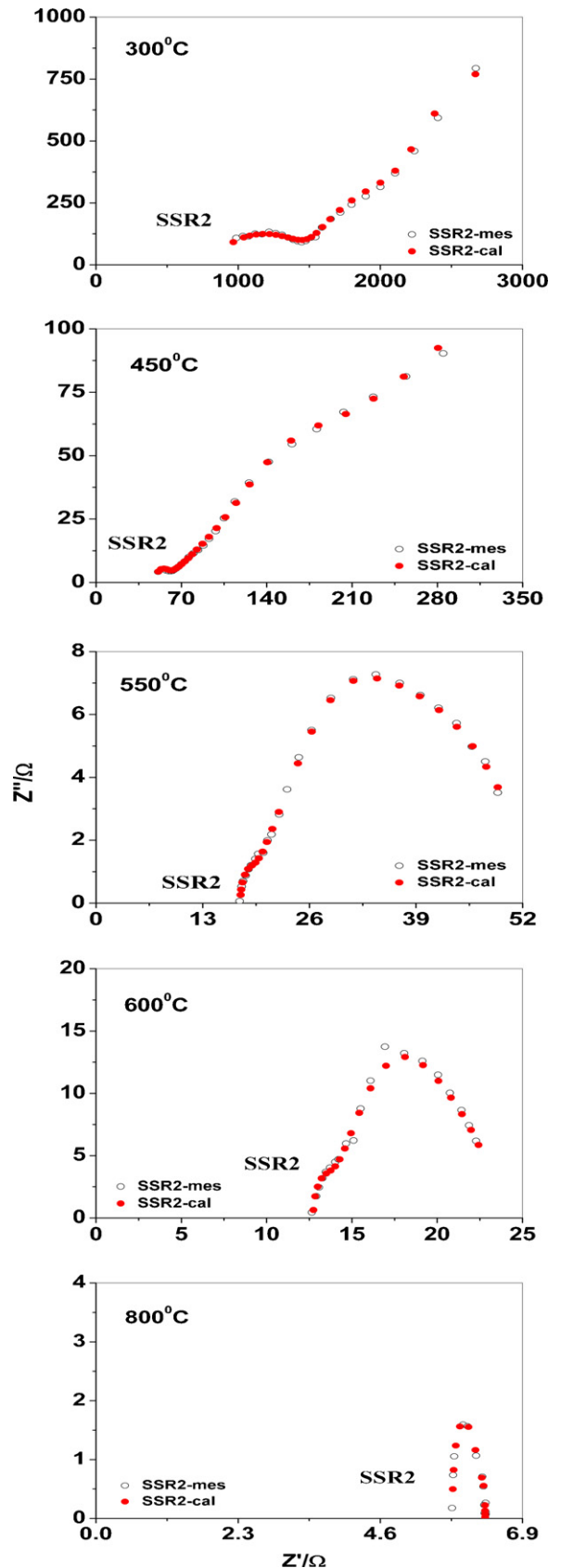
Fig. 3. Representative AC impedance spectra from 250 to 900 °C of the LSGM prepared by solid state reaction (SSR2).
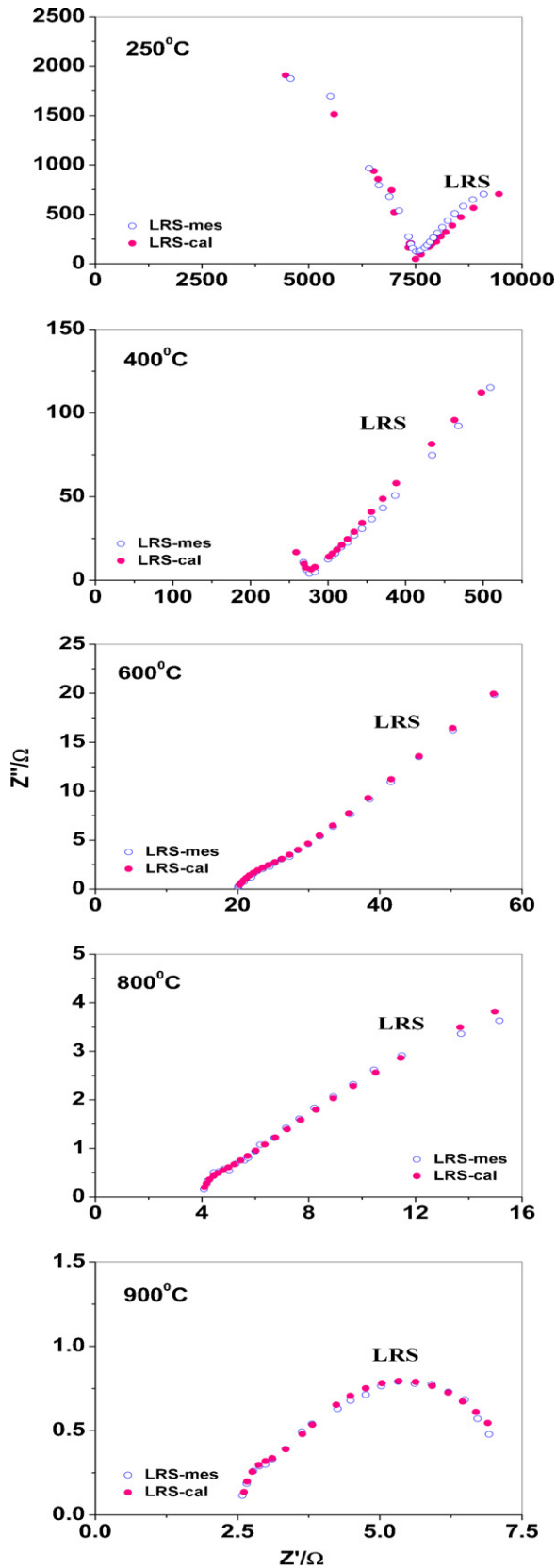
Fig. 4. Representative AC impedance spectra from 250 to 900 °C of the LSGM prepared by laser rapid solidification.
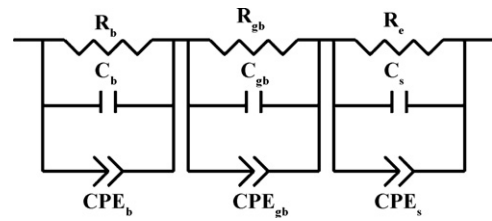

Fig. 5. Equivalent circuit for LSGM electrolyte, where R_b, R_{gb} and R_e are the electrical resistance of grain, grain boundary and electrolyte/electrode interface, respectively.

grindings (denoted as SSR2). The densities of the sintered samples were measured via the Archimedes method.

The samples were analyzed by XRD with an X'Pert PRO X-Ray Diffractometer at room temperature. Their microstructures were studied with a JSM-6700F scanning electron microscope (SEM). The laser sintered bars were re-melted by laser and polished to cuboids with 7.26 mm × 7.00 mm × 2.76 mm and the samples SSR1 were polished to 6.50 mm × 4.22 mm × 1.30 mm and SSR2 to 11.80 mm in diameter and 2.60 mm in thickness for electrical measurements. The electrical conductivities were measured in air as a function of temperature (250–950 °C) by AC impedance spectra with Pastat 2273 (Princeton Applied Research). The range of ac frequency is 0.1 Hz to 10^6 Hz. Platinum paste was fired on opposite sides of the pellets as the electrodes.

3. Results and discussion

Fig. 1a and b shows the XRD patterns of the LSGM samples SSR1 and SSR2 synthesized by solid state reactions, respectively. It is seen that the sample synthesized by solid state reaction by calcining at 1200 °C for 24 h and at 1400 °C for 6 h still contains a little amount of secondary phases of $LaSrGaO_4$ and $LaSrGa_3O_7$ and unreacted $SrCO_3$ due to lower sintering temperature (SSR1, Fig. 1a). It was noted that $LaSrGa_3O_7$ did not vanish even sintered at 1500 °C for 15 h [19]. Higher sintering temperatures (at 1250 °C for 10 h, 1500 °C for 6 h and 1600 °C for 2 h ordinally) with intermediate grindings are required for the disappearance of the secondary phases as indicated in Fig. 1b (sample SSR2). Fig. 1c–g shows the XRD patterns of the samples synthesized by laser rapid solidification with 800 W (c), 1000 W (d) and 1100 W (e) laser power at 1 mm s^{-1} scan speed, and 1100 W at 0.6 mm s^{-1} (g) and 2 mm s^{-1} (f) scan speed, respectively. The XRD results indicate that the amount of the secondary phases $LaSrGa_3O_7$ and $LaSrGaO_4$ reduces with increasing laser power and decreasing scan speed (Fig. 1c, d, and f) and LSGM samples with high purity can be easily prepared with laser power around 1100 W at a scan speed about 1 mm s^{-1} (Fig. 1e and g). A distinct feature of the
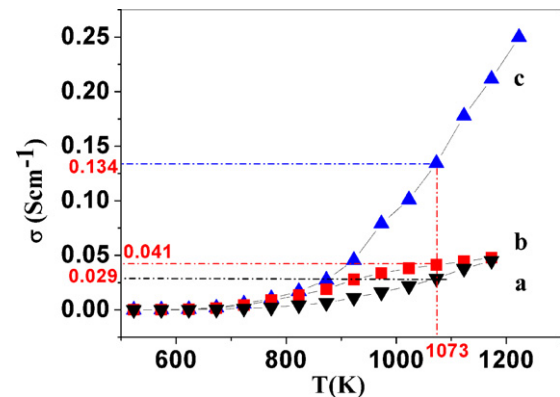

Fig. 6. The total conductivities plots of the LSGM electrolytes: (a) SSR1 and (b) SSR2 prepared by solid state reactions and (c) by LRS.

Table 1
Electrical properties and relative density of the LSGM samples prepared by solid state reactions (SSR) and laser rapid solidification (LRS).

Total conductivity (S cm^{-1})				Activation energy (eV) and Rel. density			
Temperature (°C)	SSR1	SSR2	LRS	Temperature (°C)	SSR1	SSR2	LRS
600	0.007	0.019	0.027	250–400	0.72	0.76	0.72
700	0.016	0.034	0.079	400–650	0.67	0.66	0.71
800	0.029	0.041	0.134	650–900	0.61	0.28	0.63
900	0.045	0.048	0.212	Rel. density (%)	75.0	96.9	98.5

laser synthetic route is rapid. With this technique a sample can be produced within a few seconds.

The electrical properties of the samples prepared by LRS are studied and compared with those of the samples synthesized by solid state reactions. Fig. 2 shows a typical impedance spectrum of the sample SSR2 at 250 °C. The higher, medium and lower frequency arcs represent the intragrain (R_b), grain boundary (R_{gb}) and electrode (R_e) responses, respectively [26–28]. The total resistance of the bulk, which is indicated by the vertical line in Fig. 2, is thus the sum of R_b and R_{gb}. Figs. 3 and 4 show some of the measured and calculated impedance spectra for the samples by solid state reactions (SSR2) and by LRS, respectively. It is evident from Figs. 2–4 that the grain boundary resistance of LSGMs synthesized by LRS decreases much more rapidly than that by solid state reaction with increasing temperature.

The conductivities can be calculated by fitting experimental data according to equivalent circuits comprising of a series of resistances R, capacitances C, and CPE (constant phase element) in series and/or in parallel as shown in Fig. 5. The electrolyte resistance R, sum of grain resistance R_b and grain boundary resistance R_{gb} can be calculated by fitting impedance spectra using ZSimpWin 3.0 software. The conductivity σ can then be calculated from:

$$\sigma = \frac{L}{RA} \qquad (1)$$

where L is the thickness and A is the area of the electrolyte sample. Fig. 6 shows the calculated total conductivities of the samples synthesized by LRS and SSRs. It is found that the conductivities of the sample synthesized by LRS are superior to those of both samples by solid state reactions at any temperatures and the conductivities of 0.027, 0.079 and 0.134 S cm^{-1} obtained at 600, 700 and 800 °C (see also Table 1 below), respectively, are very close to the best reported values for this composition [20,29,30]. While a saturation effect in conductivity appears at temperatures above ~650 °C for the sample SSR2, the conductivity increases almost linearly with temperature for the sample synthesized by LRS and no saturation occurs at even the highest measured temperature.

Fig. 7 presents the Arrhenius plots of the total conductivities for the LSGM samples prepared by solid state reactions and LRS, respectively. The Arrhenius plots exhibit different slopes in the low and high temperature regions and the transitional temperature is around 450 °C. Another turning point for SSR2 and the sample by LRS appear at about 600–700 °C which is in accordance with the previous results [19,20,31]. The turning points imply an activation energy changes at these temperatures. In Table 1 we summarize the total conductivities, activation energies at different temperature ranges of the samples prepared by solid state reactions and LRS, respectively. Table 1 shows that the activation energy decreases with increasing temperature and it does not have much difference for all the samples in the low temperature range. However, the sample SSR2 exhibits much lower activation energy in the high temperature range (650–900 °C) due to the saturation effect mentioned above.

The main transport mechanism in magnesium- and strontium-doped LaGaO$_3$ (LSGM) is the migration of oxygen vacancies which are formed in the following defect reaction:

$$2SrO \xrightarrow{La_2O_3} 2Sr'_{La} + \ddot{V}_o + 2O_o^x, \quad 2MgO \xrightarrow{Ga_2O_3} 2Mg'_{Ga} + \ddot{V}_o + 2O_o^x \qquad (2)$$
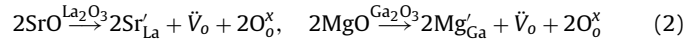
here $\ddot{V}_o$ represents oxygen vacancy and O_o^x is the oxygen in the crystal lattice. The activation energy normally includes the dissociation energy and the migration energy of oxygen vacancies. At lower temperatures, the oxygen vacancies are trapped out into ordered-vacancy clusters due to Coulombic interaction between the doped cations and vacancies [18,20,30,31] and they hence need a higher activation energy to dissociate. They can be progressively dissolved into the matrix of the oxygen sites with increasing temperature, leading to a lowering of the activation energy [18,20,30,31].

The electrical conductivity (σ) is proportional to the concentration of charge carriers n (cm^{-3}), the charge of each carrier q (coulombs) and their mobility μ (cm^2 s^{-1} V^{-1}) [32–34], i.e.

$$\sigma = nq\mu \qquad (3)$$

A higher conductivity may imply a higher concentration and/or a higher mobility of the oxygen vacancies in the sample. The measured relative densities of the samples are 75.0% (SSR1), 96.7% (SSR2) and 98.5% (LRS) (see Table 1), respectively. Although the relative density could be one of the reasons for the differences in conductivity of the three samples, it cannot explain the large difference in conductivity of the samples SSR2 and LRS since their relative densities are very close. This means that the difference in carrier mobility must be the main cause in the difference of conductivity. The mobility μ can be expressed as:

$$\mu = \frac{q\tau}{m^*} \qquad (4)$$

where τ is the mean free time and m^* is the effective mass of charge carriers. The mean free time τ is mainly affected by the scattering of the lattice vibration, impurities and grain boundaries.

In order to understand the super conductivity of the sample by LRS, we show in Figs. 8 and 9 the typical SEM images of the surface and fractured cross-section of the LSGM samples prepared by LRS and solid state reactions, respectively. It is evident that
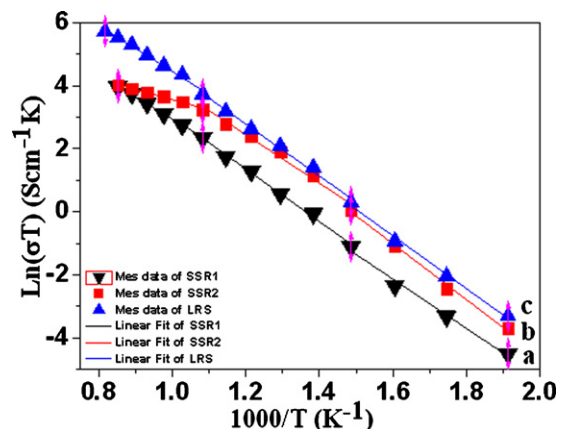

Fig. 7. Arrhenius plot of total conductivities for LSGM electrolyte prepared by two different methods: (a) LSGM/SSR1; (b) LSGM/SSR2; (c) LSGM/LRS.
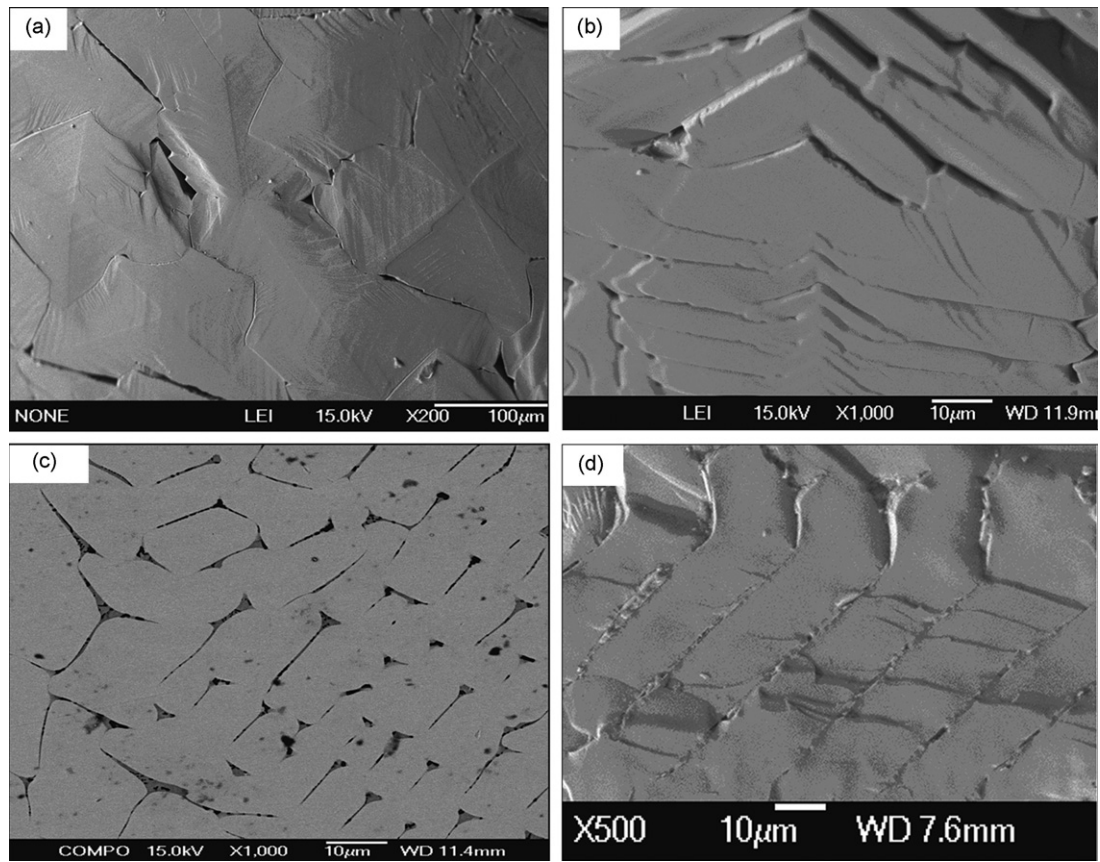
Fig. 8. SEM images of the LSGM samples prepared by LRS: (a and b) surface; (c) polished surface; (d) fractured cross-section.
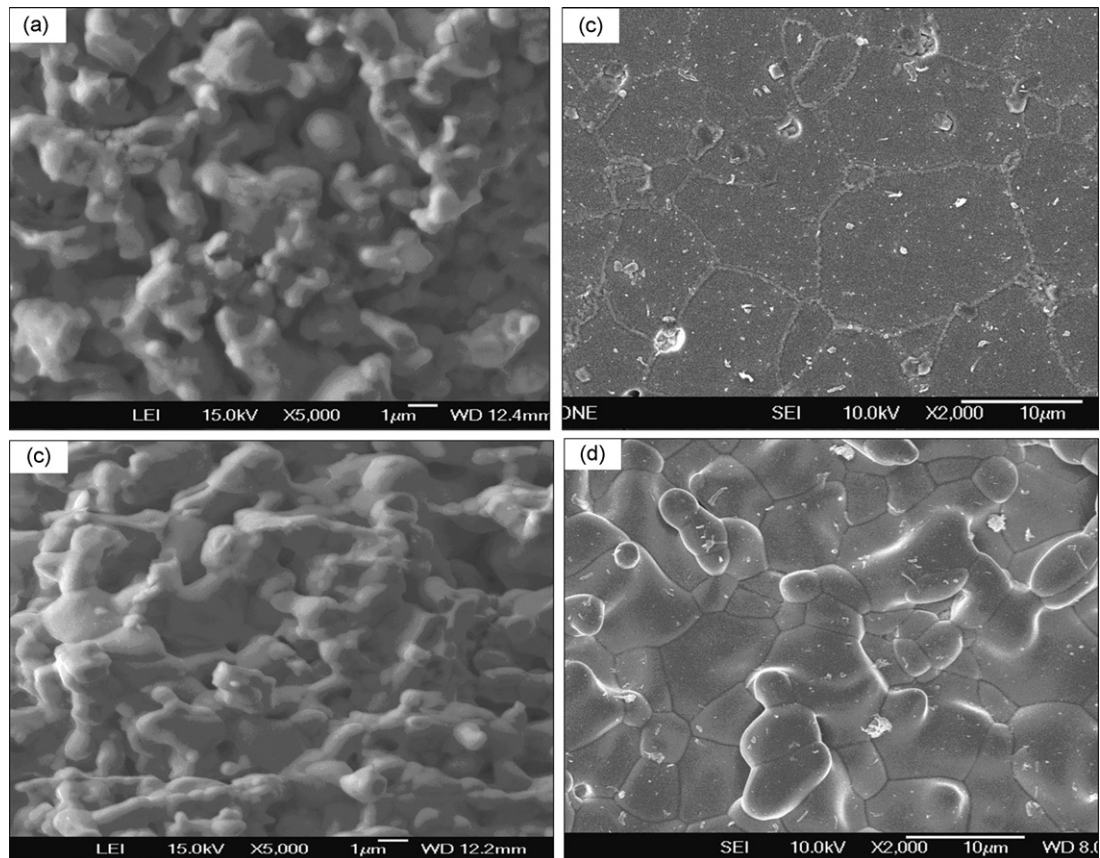

Fig. 9. SEM images of the LSGM samples prepared by solid state reactions: (a) surface/SSR1; (b) surface/SSR2; (c) fractured cross-section/SSR1; (d) fractured cross-section/SSR2.

the microstructure of the sample by LRS is characterized by relatively orderly arranged and densely packed blocks while the sample SSR1 (Fig. 9a and c) prepared by solid state reaction is composed of irregular shaped particles with many large poles and SSR2 (Fig. 9b and d) consists of densely packed globose grains. The average grain sizes of LRS SSR1 and SSR2 are about 10–20 μm (with length exceeding 20 μm), 1–3 μm and 5–10 μm, respectively. The unique microstructures of the sample by LRS, should account mainly for its superior electrical properties to those of the samples by solid state reactions. The relatively oriented and densely packed ridge-like grains with large and regular sizes in the sample by LRS greatly reduce the scattering probabilities and thus increase the mean free path or the mean free time τ of charge carriers during the drift motion. In addition to the lower concentrations of oxygen vacancies as indicated by the relative density measurements, the smaller grain sizes in SSR2 and numerous poles, impurities and smallest grain sizes in SSR1 lead to higher scattering probabilities and lower mean free time of the carriers, making them the poorer and poorest in conductivity, respectively.

The laser rapid solidification distinguishes itself from those of solid state reactions and wet chemical routes in mechanism. In the laser synthetic route, the raw materials were heated to melt immediately upon illumination of the laser beam and formed a molten pool where the chemical reaction took place. The products solidified rapidly as the laser beam moved ahead. It can be speculated from the appearances and SEM images that the starting materials were sufficiently molten in the molten pool. A temperature of above 2830 °C in the molten pool is expected since the melting points of the raw materials La_2O_3, $SrCO_3$, Ga_2O_3 and MgO are about 2315, 1497, 1740 and 2827 °C, respectively. The sufficiently high temperature ensured sufficient melting of the raw materials and consequently rapid and uniform reactions. As the laser energy was absorbed by the top layer of the raw materials, heat transfer in a sample was mainly directed from the top surface to the bottom and also governed by the moving direction of the laser beam. The unique microstructures of the samples produced in the laser synthetic route can be attributed to the relatively oriented crystalline growth governed by heat transfer directions in the liquid droplet-like molten pool.

4. Conclusion

We developed a new and rapid synthetic route for the synthesis of $La_{0.9}Sr_{0.1}Ga_{0.8}Mg_{0.2}O_{3-\delta}$ by rapid solidification with a CO_2 laser. Pure perovskite LSGM phase can be produced within a few seconds with this method under optimized synthetic conditions. The optimum conditions for the synthesis of $La_{0.9}Sr_{0.1}Ga_{0.8}Mg_{0.2}O_{3-\delta}$ are around 1000–1100 W laser power and 1 mm s^{-1} scan speed. The materials solidified in densely packed and relatively ordered ridge-like blocks with relative density of 98.5%. The unique microstructures are attributed to the oriented growth of crystalline in the molten pool dictated by heat transfer directions. The unique microstructures together with the larger grain sizes and higher density make the sample exhibit superior electrical properties as fuel cell electrolyte. It is found that the sample synthesized by LRS has much higher conductivities at any temperatures measured than those of the sample synthesized by solid state reactions with similar purity and density. Particularly in the high temperature regions, while the sample SSR2 shows a saturation effect at temperatures above ∼650 °C, the sample synthesized by LRS increases almost linearly with temperature and no saturation effect appears at even the highest measured temperature. The excellent electrical properties suggest a higher concentration and mobility of the oxygen vacancies in the sample synthesized by LRS than in those synthesized by solid state reactions which are confirmed by relative density measurements and microstructure observations.

References

[1] C. Compson, M. Liu, Solid State Ionics 177 (2006) 367–375.
[2] R.A. George, N.F. Bessette, J. Power Sources 71 (1998) 131–137.
[3] I. Minoru, M. Atsushi, Solid State Ionics 104 (1997) 303–310.
[4] M. Lang, R. Henne, S. Schaper, G. Schiller, J. Therm. Spray Technol. 10 (4) (2001) 618–625.
[5] N.Q. Zhang, K.N. Sun, D.R. Zhou, D.C. Jia, J. Rare Earths 24 (2006) 90–92.
[6] E. Gomes, F.M.B. Marques, F.M. Figueiredo, Solid State Ionics 179 (2008) 1325–1328.
[7] P. Datta, P. Majewski, F. Aldinger, J. Alloys Compd. 438 (2007) 232–237.
[8] P. Datta, P. Majewski, F. Aldinger, Mater. Chem. Phys. 102 (2007) 240–244.
[9] P. Datta, P. Majewski, F. Aldinger, Mater. Res. Bull. 43 (2008) 1–8.
[10] R. Polini, A. Falsetti, E. Traversa, O. Scḧaf, P. Knauth, J. Eur. Ceram. Soc. 27 (2007) 4291–4296.
[11] C. Oncel, B. Ozkaya, M.A. Gulgun, J. Eur. Ceram. Soc. 27 (2007) 599–604.
[12] N.S. Chae, K.S. Park, Y.S. Yoon, I.S. Yoo, J.S. Kim, H.H. Yoon, Colloids Surf. A: Physicochem. Eng. Aspects 313–314 (2008) 154–157.
[13] T.Y. Chen, K.Z. Fung, J. Eur. Ceram. Soc. 28 (2008) 803–810.
[14] D. Lee, J.H. Han, Y. Chun, R.H. Song, D.R. Shin, J. Power Sources 166 (2007) 35–40.
[15] S. Li, B. Bergman, J. Eur. Ceram. Soc. 29 (2009) 1139–1146.
[16] Y.L. Zhai, C. Ye, J.Z. Xiao, L. Dai, J. Power Sources 163 (2006) 316–322.
[17] Y.L. Zhai, C. Ye, F. Xia, J.Z. Xiao, L. Dai, Y.F. Yang, Y.Q. Wang, J. Power Sources 162 (2006) 146–150.
[18] M. Shi, N. Liu, Y.D. Xu, Y.P. Yuan, P. Majewski, F. Aldinger, J. Alloys Compd. 425 (2006) 348–352.
[19] N. Liu, Y.P. Yuan, P. Majewski, F. Aldinger, Mater. Res. Bull. 41 (2006) 461–468.
[20] K.Q. Huang, R.S. Tichy, J.B. Goodenough, J. Am. Ceram. Soc. 81 (1998) 2565–2575.
[21] E.J. Liang, T.A. Wu, B. Yuan, M.J. Chao, W.F. Zhang, J. Phys. D: Appl. Phys. 40 (2007) 3219–3223.
[22] E.J. Liang, S.H. Wang, T.A. Wu, M.J. Chao, B. Yuan, W.F. Zhang, J. Raman Spectrosc. 38 (2007) 1186–1192.
[23] E.J. Liang, H.L. Huo, J.P. Wang, M.J. Chao, J. Phys. Chem. C 112 (2008) 6577–6581.
[24] E.J. Liang, H.L. Huo, Z. Wang, M.J. Chao, J.P. Wang, Solid State Sci. 11 (2009) 139–143.
[25] E.J. Liang, J.P. Wang, E.M. Xu, Z.Y. Du, M.J. Chao, J. Raman Spectrosc. 39 (2008) 887–892.
[26] J.R. Macdonald, Impedance Spectroscopy, Wiley, NY, 1987.
[27] J.V. Herle, A.J. McEvoy, K.R. Thampi, J. Mater. Sci. 29 (1994) 3691–3701.
[28] I. Kosacki, H.U. Anderson, Y. Mizutani, K. Ukai, Solid State Ionics 152/153 (2002) 431–438.
[29] J.W. Stevenson, T.R. Armstrong, L.R. Pederson, J. Li, C.A. Lewinsohn, S. Baskaran, Solid State Ionics 113–115 (1998) 571–583.
[30] Z.C. Li, H. Zhang, B. Bergmana, X. Zou, J. Eur. Ceram. Soc. 26 (2006) 2357–2364.
[31] B.W. Liu, Y. Zhang, J. Alloys Compd. 458 (2008) 383–389.
[32] H.L. Tuller, in: O.T. Sørensen (Ed.), Nonstoichiometric Oxides, Academic Press, New York, 1981.
[33] R.W. Vest, J.M. Honing, in: N.M. Tallan (Ed.), Electrical Conductivity in Ceramics and Glass, Marcel Dekker, New York, 1974.
[34] S.Q. Hui, J. Roller, S. Yick, X.G. Zhang, C. Dec'es-Petit, Y.S. Xie, R. Maric, D. Ghosh, J. Power Sources 172 (2007) 493–502.